INTL JOURNAL OF ELECTRONICS AND TELECOMMUNICATIONS, 2021, VOL. 67, NO. 4, PP. 570-577
Manuscript received August 13, 2021; revised November, 2021 DOI: 10.24425/ijet.2021.137848

Design and Analysis of a Hybrid Circularly Polarized Multi-Band MIMO Antenna for Sub 6 GHz Applications

S. Salma, Habibulla Khan, B. T. P. Madhav, D. Ram Sandeep, and M. Suman

***Abstract*—In this article, a hybrid circularly polarized Multiple-Input Multiple-Output (MIMO) antenna for multi-band operation from 2.3 to 9.2 GHz with an impedance bandwidth of 7 GHz is proposed and investigated experimentally. The designed MIMO antenna model has a compact size of 20mm×40mm×1.6mm on the FR-4 substrate. The microstrip feed of the proposed slot antenna consists of a tapered structure, and the radiating element consists of the inverted L- shaped slots, which were opened on both sides of the radiating elements to introduce notches at the sub-6 GHz frequencies. L-shaped stubs are also introduced on another side of the substrate in the common ground plane to attain high isolation between the radiating elements of the proposed antenna. In the operating band from 2.3 to 9.2 GHz, isolation of less than -20 dB is achieved by the proposed model. The performance of the circularly polarized MIMO antenna in terms of RHCP and LHCP radiation patterns, axial ratio, surface current distributions, isolation between the ports, diversity gain (DG), envelope correlation coefficient (ECC), total active reflection coefficient (TARC), and peak gain are studied and presented in this work. The obtained characteristics of the proposed antenna make it suitable for sub-6-GHz frequency applications.**

***Keywords*—Axial Ratio (AR), Circular Polarization, MIMO Antenna, SEA (Single Element Antenna)**

I. INTRODUCTION

WHEN compared to Single Input Single Output (SISO) systems without increasing the total power consumption and bandwidth, one of the possible ways to increase transmission capacity and reliability of the system is Multi-Input Multi-Output (MIMO) techniques. The significant parameter that needed to be considered while developing a MIMO antenna system in a transmitter or receiver is the low mutual coupling. The size of the MIMO antenna is the primary constraint for antenna developers. The compact MIMO system is packing of the antennas nearer to each other, which unavoidably leads to remarkable mutual coupling between them, subsequently depreciates the MIMO antenna diversity performance. So, the main problem that has to confront while actualizing a MIMO antenna with compact size is the mutual coupling in between the patch elements. Sub 6 GHz spectrum has been allocated as the next generation communication applications, like china allocated 3.3-3.6 GHz and 4.8-5.0 GHz, in the US its 600 MHz and 3.7-4.2 GHz. In the European Union, it's the 700 MHz and 3.4-3.8 GHz. In the recent past, many antennas were developed by the designers, set to operate under sub-6 GHz frequencies to meet the bands of 5G and upcoming mobile communication bands.

To minimize the mutual coupling and to attain high isolation for the MIMO antenna system, several methods were proposed. The literature review shows that in [1], the authors used a neutralization line to resolve this problem, and it is realized between the radiating element of the designed MIMO antenna.

In [2], the authors proposed a UWB MIMO and achieved -20 dB isolation between the radiating elements using F-shaped stubs at the ground plane. In [3], a MIMO antenna on polydimethylsiloxane (PDMS) substrate is developed. The use of PDMS technology achieved the isolation of -30 dB and also showed promising features in terms of optical transparency, environmental resistance, and flexibility. In [4], the antenna developers reduced mutual coupling by using parasitic elements. A double coupling path is realized by using the parasitic elements, and this path creates a reverse coupling effect to suppress the mutual coupling. In [5], a pair of micro-machined Meander-Line (ML) slots are inserted between closely spaced two patches on the ground plane in a complementary symmetric point fashion to reduce mutual coupling without any mismatch in the resonant frequency.

Circularly polarized (CP) antennas have a unique polarization scheme, and they are known for their flexibility in the angle of orientation between the transmitter and receiver; also, they can reduce the multipath distortions. Due to these advancements, CP MIMO antennas gained popularity, and a MIMO ground radiation antenna is reported in [6]. The CP is achieved by controlling the phase difference between the simultaneously excited vertical and horizontal modes of the ground plane, by utilizing a spring-loaded metal strip. In [7], the authors proposed a carefully packed MIMO antenna with polarized diversity, and the CP was achieved by placing an open-ended, hook-shaped stub in the ground plane.

In this paper, a hybrid CP multi-band MIMO antenna for sub-6 GHz applications was presented. It has a compact size of 20×40 mm^2. It comprises of a polygon-shaped radiating element with three L-shaped slits designed as for notched filter structures to cover the bandwidth of 2.3 GHz to 9.2 GHz operating frequencies.

We thank DST for their technical support by project SR/FST/ET-II/2019/450.

S. Salma, and D. Ram Sandeep are with Dept. of ECE, Koneru Lakshmaiah Education Foundation, AP, India (email: salmaa.syed24@gmail.com, askram91@gmail.com).

Habibulla khan, B. T. P Madhav, and M. Suman are with Dept. of ECE, Koneru Lakshmaiah Education Foundation, AP, India (email: {habibulla, btpmadhav, suman.maloji} @kluniversity.in).

II. Design and Evolution of SEA

The proposed antenna is evolved from a Single Element Antenna (SEA) to a multi-band MIMO antenna. Both the antennas are designed on commercially available FR-4 substrate, with a loss tangent of 0.02, the relative permittivity of 4.4, and a thickness of 1.6mm. The antenna's dimensional parameters are optimized using Ansys HFSS 19.0. The overall dimensions of the SEA are 20 x 20 x 1.6 mm^3. The MIMO antenna patch is evolved by duplication of a single element patch, and the designed MIMO antenna footprints are 20 × 40 x 1.6 mm^3.

The evolution of the SEA is illustrated in Fig.1. In iteration-1, the patch comprises polygon structure as a radiating element (which is inspired by the air traffic control tower) with the full ground structure is shown in Fig.1(a). This design is resonating around 9 GHz with a reflection coefficient of less than -10 dB. In iteration-2, as shown in Fig.1(b), three triangular protrusions towards the ground were made on both sides of the patch to make changes in the path surface currents, and the half ground structure was considered in the ground plane. This model resonated at 6.5 GHz with a return loss of -15dB. In Iteration-3, as shown in Fig.1(c) Inverted L-shaped slots are opened on both sides of the patch structure to alter the surface currents moving around the slots. A pillar-like stub is placed on the right side of the ground to resonate the antenna at lower frequencies. This model resonated at 4.5, 7 GHz with a return loss of -13,-25 dB. To furtherly alter the surface currents and resonate it in lower frequencies, two more inverted L shaped slots are opened on either side to the patch, as shown in Fig.1(d). The ground structure is modified from iteration-3 by adding a staircase like DGS to allow the patch elements to radiate more and also to recreates the same possible effects of the tower structure in that iteration-3. The S11 parameter of SEA is shown in Fig.2. It is observed that the iteration-4 has good resonating sub-6 GHz frequencies with a return loss of 25.7dB. Therefore, the iteration-4 of the SEA is further modified to a dual-element MIMO antenna. The overall dimensions of SEA with units (mm) are as follows: LSub1=20, WSub1=20, h=1.6, Lf=10, Wf=4, Lp= 9, WP= 18, Lp= 9, Wg= 20, Lg=10, Wsg1=5, Lsg1=19, WS1= 4, LS1= 3, Wsg2= 2, Lsg2= 11, Wsg3=6, Lsg3= 3, WS2= 5, LS2= 4, WS3= 7, LS3=6, G1= 0. 5, G2= 0. 3, G3= 0. 3.

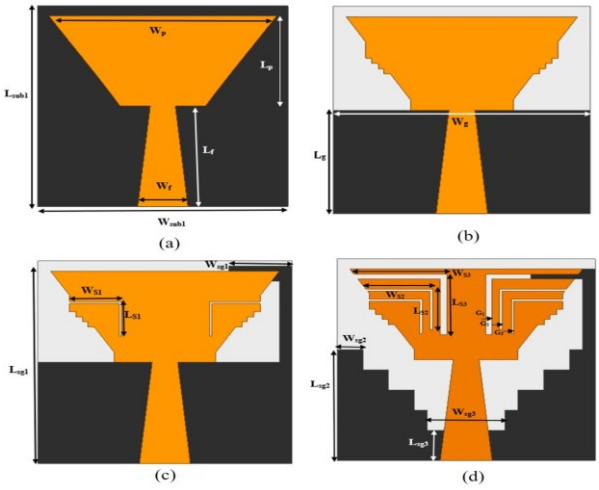

Fig. 1. SEA Geometry

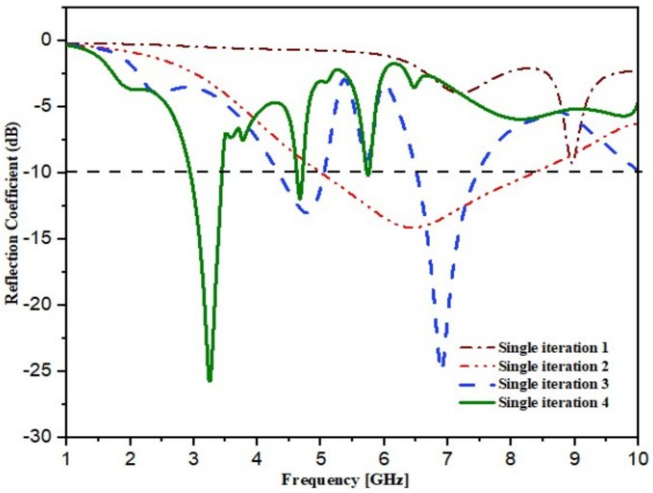

Fig. 2. SEA Reflection Coefficient

III. Design and Evolution of MIMO Antenna

The dual-element MIMO antenna iterations are illustrated in Fig.3. The iteration-1 shows the evolution of the patch, and it is developed by placing another identical radiation element next to the existing one in the single element antenna against the full ground structure is as shown in Fig.3(a). The overall dimensions of the substrate changes are 20×40×1.6 mm^3. As shown in Fig.4, this model resonated at 3.3, 3.5, 4.5, 5.3, and 7.5 GHz with a return loss of -23, -15, -26, -14, -15 dB. In iteration-2, the patch is kept unmodified as in iteration-1, and a half ground structure is considered in the ground plane is as shown in Fig.3(b). This design does not resonate in the sub-6 GHz bands because of the half ground structure, which maximizes the mutual coupling effect between the radiating element.

In iteration-3, as shown in Fig.3(c), to furtherly reduce the mutual coupling effects, a rectangular stub with extended arms is added to the center of the half ground structure. This model intended to alter the surface current directions in the patch and to attract the currents towards the terminals of the rectangular pillar stubs. This modification reduces the mutual coupling between them and resonating at frequencies 3, 3.5, and 6.2 GHz with a return loss of -13, -18, and -15 dB.

To study the possible effects of DGS, iteration-4 is analyzed. As shown in Fig.3(d), the ground plane is modified by removing the elements to make a staircase structure at the center. The dimension, such as height and length of each step is given below. This model altered the movements of surface currents by attracting the currents towards the bottom center of the patch and achieved the isolation of -18 dB. This model resonated at 4.0, 4.5, 5.2, 5.6, and a wideband between 6-8.7GHz frequencies with a return loss of -12, -18, -27, -24, and -22dB.

From the above study, the DGS with a staircase-like structure resonated better with good isolation between the radiating elements. This design was furtherly considered to alter both the patch and ground elements by assigning and removing some more elements to resonate the antenna in sub 6 GHz frequencies with the CP feature in maximum operating bands and also to achieve good isolation. The overall dimensions of MIMO iterations with units (mm) are as follows: LSub2=20, WSub2=40, Lsg4=40, Wsg4=9, Lsg5= 10, Wsg5= 12, Lsg6=2,

Wsg6= 12. The SEA and MIMO structures are designed by compact size with the basic lower resonant frequency equation (1, 2, and 3) as follows [8],

$$f_r = \frac{14.4}{(L_1)+(L_2)+g+\frac{A_{g1}}{2\pi\sqrt{\varepsilon_r}+1}+\frac{A_{g2}}{2\pi\sqrt{\varepsilon_r}+1}} \quad (1)$$

$$A_{g1} = 2\left[\left(L_1 - L_{sg7}\right)W_{sg8}L_{sg9}\right]+W_{sg7}L_{sg7} - W_{sg9}\left(Lsg7 - L_{Sub3}\right) \quad (2)$$

$$A_{g2} = W_pL_p+\frac{1}{2}\left[W_p(L_p - L_{s8})\right]+W_fL_f \quad (3)$$

Where ***Ag1*** and ***Ag2*** in the area of the radiating element and ground plane, ***L1***= Lsg7 + Lsg8 and ***L2***=Lsg7 is the length of the radiating structure and the ground plane, ***g*** = Lf - Lsg7 indicates the radiating element and ground plane gap.

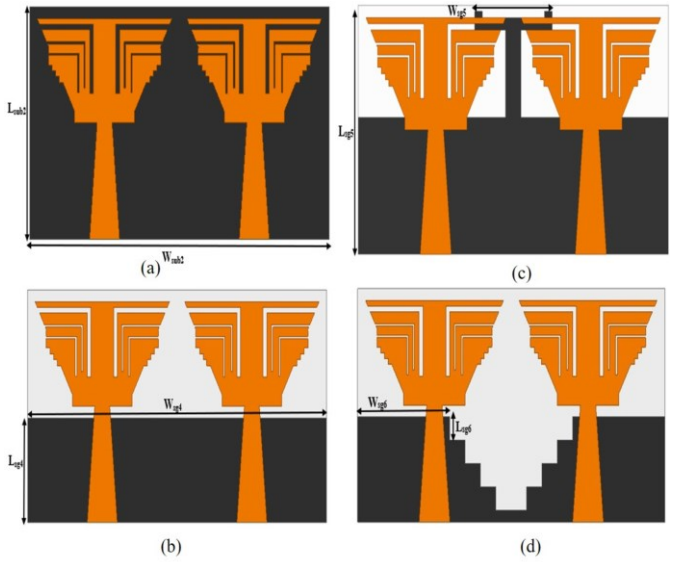

Fig. 3. MIMO Antenna Geometry

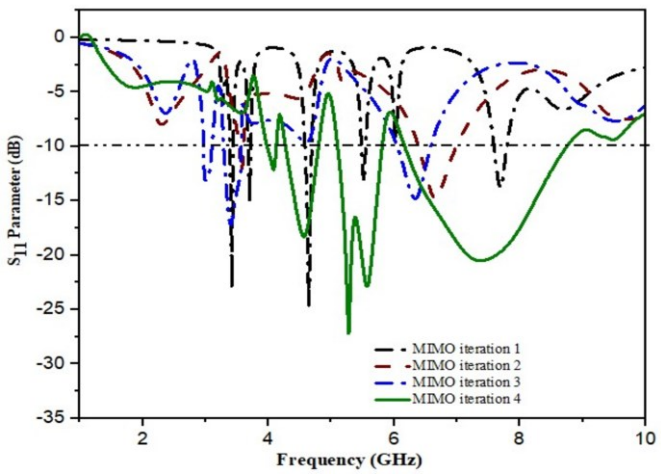

Fig. 4. MIMO Antenna Reflection Coefficient

VI. Proposed Multiband MIMO Design

In this Proposed model, as shown in Fig.5(a) and 5(b), inverted T-shaped slots were opened in the radiating elements of the patch. These slots aid the surface currents to distribute equally on both sides. As the pathway decreases, the currents diverge in all sides and help to spread around the available spaces, and this is the final patch structure. The ground plane is built using the ground structure from the MIMO iteration-4, which is shown in Fig. 5(c). Initially, the staircase structure was considered and started adding rectangular and square cubes up to half of the ground plane. This pattern was developed to distribute the surface currents in the ground plane between the sharp points that are formed by joining these square and rectangular blocks. A rectangular tower-like stub with a horizontal rectangular slab was placed on the of this structure.

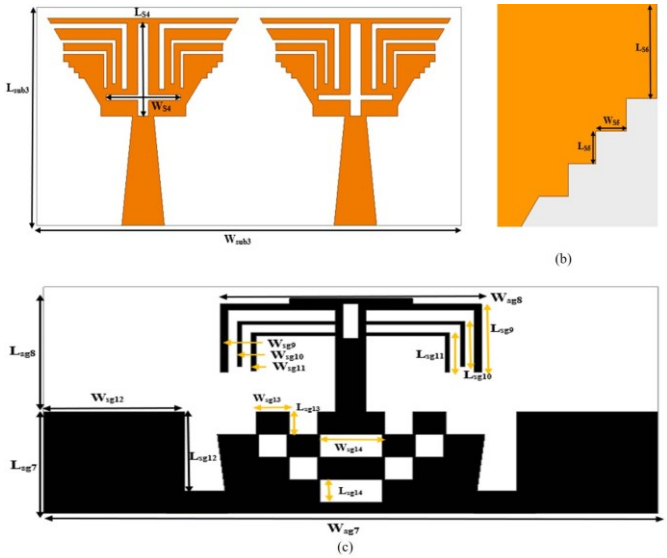

Fig. 5. Proposed Multi-band MIMO antenna (a) Top view (b) Staircase view, (c) Bottom view

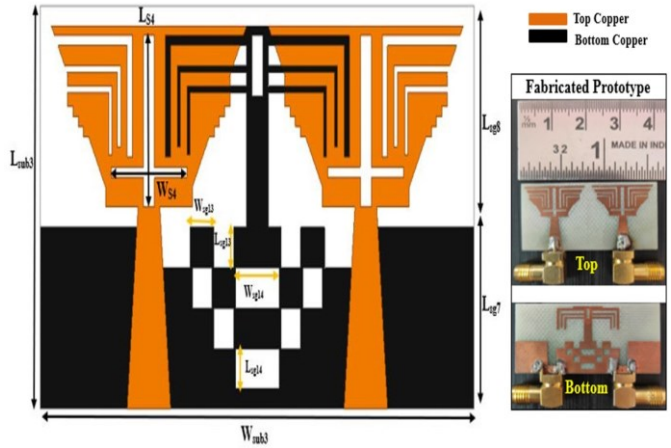

Fig. 6. Overall Proposed Multi-band MIMO antenna with the prototype

Finger-like extensions are drawn from the rectangular slab, which is exactly of the same sizes of the inverted L- shaped slits of the patch. These alterations ate made to increase the fringing effect and to minimize the mutual-coupling between the radiating elements. To furtherly increase, this effect a null space is created at the bottom of the finger-like extensions. This design

resonates at notch bands in 2.3, 3.5, 3.9, 4.5 GHz, and with wide bands between 4.8-6.4 and 7.2-9 GHz and achieved CP in 6 operating bands. The overall dimensions of the multi-band MIMO antenna (mm) are as follows and shown in Fig.6: LSub3=20, WSub3=40, WS4= 7, LS4= 8.5, Lsg7=22, Wsg7=9, Lsg8=10, Wsg8=17, Lsg9= 6, Wsg9=0.5, Lsg10=4, Wsg10= 0.3, Lsg11=3.4, Wsg11= 0.3, Lsg12=7, Wsg12=9, Lsg13=2, Wsg13=2, Lsg14=4, Wsg14= 2, LS5=0.5, WS5= 0.5, LS6=1.5. The L-shape slots, which act as HGWR (Half Waveguided Resonator), and its lengths, can be calculated by the equations (4, 5, and 6). The resonant frequencies of slits can be calculated by equation 7.

$$S_1 = 2(L_{S3} + G_1 + W_{S3} + G_1) \quad (4)$$

$$S_2 = 2(L2 + G_2 + W_{S2} + G_2) \quad (5)$$

$$S_3 = 2(L_{S1} + G_3 + W_{S1} + G_3) \quad (6)$$

$$f_r = \frac{C}{2(S_1 + S_2 + S_3)\sqrt{\varepsilon_{reff}}} \quad (7)$$

Where C indicating the speed of the light, and ε_{reff} is considered as an effective dielectric constant.

V. RESULTS AND ANALYSIS

A. Reflection coefficient

The proposed antenna is evaluated experimentally, and the measurements are taken in the anechoic chamber with combinational analyzer MS2037C. Fig.7 illustrates the simulated and measured S-parameters; a good agreement is observed between them. The proposed antenna resonates at 2.3GHz, (3.4-3.5 GHz), (3.8-3.9 GHz), (4.0-4.6 GHz), (4.8-6.4 GHz), (7.2-9.2 GHz) with bandwidth S11 / S22 <−10 dB and S21 / S12 < -20 dB. From Fig.7, it is observed that the simulated S11/S22 and S12/S21 are identically equal to measured results. The proposed multi-band MIMO antenna covers the impedance bandwidth of less than 7GHz from 2.3-9.2 GHz frequency. From Fig.7, it's observed that the simulated transmission coefficient from (S12=S21) is less than -20 dB with good isolation of -29dB in the operating bands. Better isolation is considered when S12 / S21 ≤-20dB. Fig.8 shows the proposed antenna prototype, which is measured using the combinational analyzer in an anechoic chamber.

B. Surface current distributions

The CP feature of the designed antenna is projected with surface currents at resonating frequencies for better understanding. Table 1 shows the surface current distribution concerning the change in phase. In each resonating frequency, they are moving circularly in the clockwise direction. The reason for this rotation can be explained as; (1) By using the tapered fed and opened inverted slots in the patch, they make to move the currents through narrow streams in a divergent circular path from one side to another.

The narrow inverted L slots of 0.3 mm width are mainly responsible for altering the current distributions; for this reason, maximum radiation can be found around them. In each resonating frequency, the surface currents movement at the 0-degree phase is towards the upward direction. Concerning the phase change of 90 degrees, they are moving towards the right-hand side. This phenomenon can be observed in all resonating frequencies. Concerning the 180-degree phase shift, the currents are moving in the downward direction in all resonating frequencies, and finally, for a 270-degree phase shift, they are moving towards the left-hand side. In a total shift in phase from the 0-360 degrees phase, they are moving circularly.

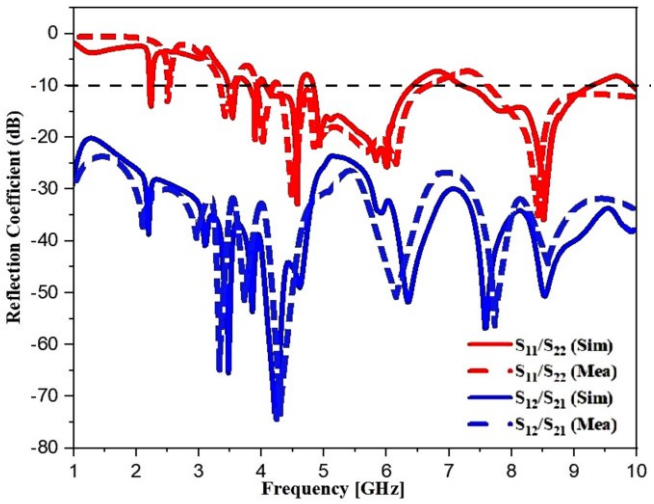

Fig. 7. Multi-band MIMO antenna S-Parameters

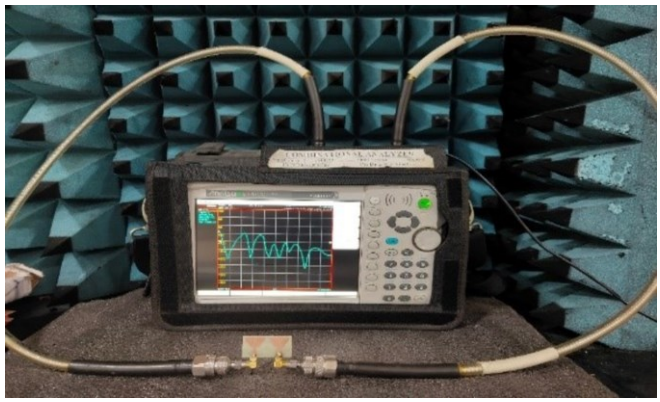

Fig. 8. Measurement setup of the proposed Multi-band MIMO antenna

C. Axial Ratio

In a polarization ellipse, the axial ratio will be taken as the ratio to the major axis to the minor axis. Ideally, its value is unity (Zero dB), which means the polarization ellipse is transformed into a circle; that is why it is called as circularly polarization. Practically its value is anywhere less than 3dB, the closer to zero, the better the axial ratios. Fig.9 illustrates the axial ratios of the proposed antenna in the boresight direction. A decent agreement can be observed between the simulation and the measurement.

The resonating bands where the axial ratios are less than 3dB are range from 2.3 GHz, (3.4-3.6 GHz), (5.0-6.1 GHz). Hence they are resonating with CP in Sub 6 GHz Communication applications such as 2.3 GHz (Wireless MAX), 3.6 GHz (Wireless LAN), 5.0 GHz (Wi-Fi), 5.3 GHz (Hyper LAN), 5.8 GHz (Industrial Scientific & Medical), and 5.9 GHz (Wireless LAN) applications.

TABLE I

SURFACE CURRENTS DISTRIBUTIONS OF THE PROPOSED MIMO CONCERNING THE CHANGE IN PHASE.

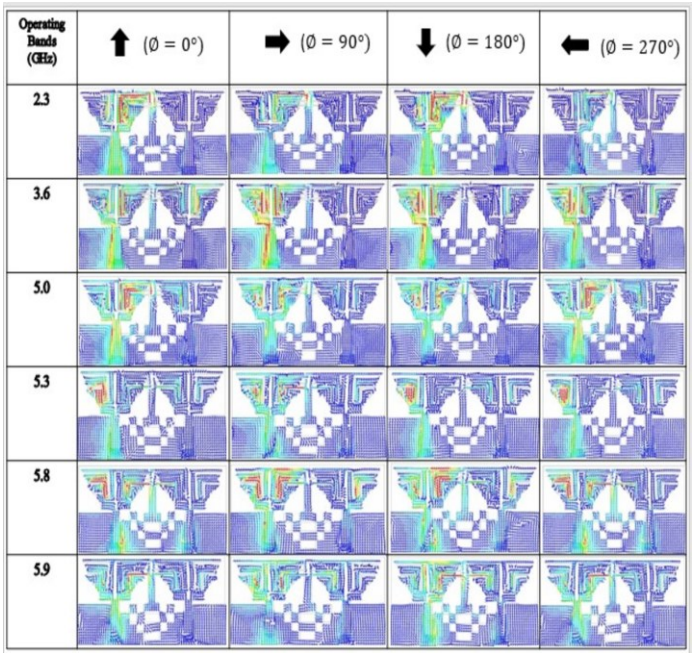

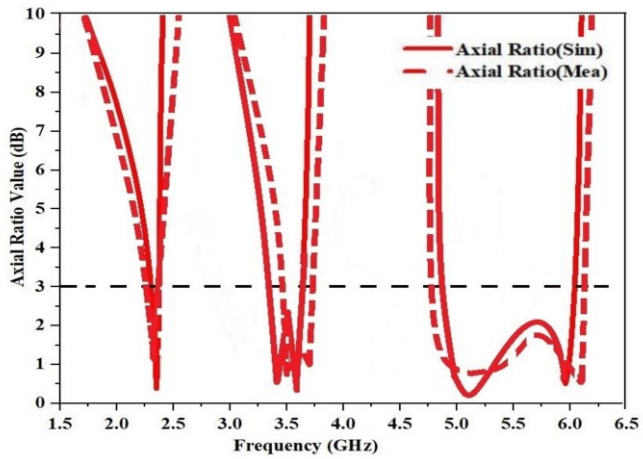

Fig. 9. Multi-band MIMO antenna axial ratios in the boresight direction

D. Radiation Patterns

Additionally, the radiation performance of the MIMO antenna model was analyzed in the anechoic chamber. A decent agreement has been observed between the simulation and measurement. The Fig.10 illustrates the RHCP (Right Hand Circular polarization) and LHCP (Left Hand Circular Polarization) on the two principal planes ($\varphi = 0°$, $\varphi = 90°$) in E and H planes of the proposed MIMO antenna.

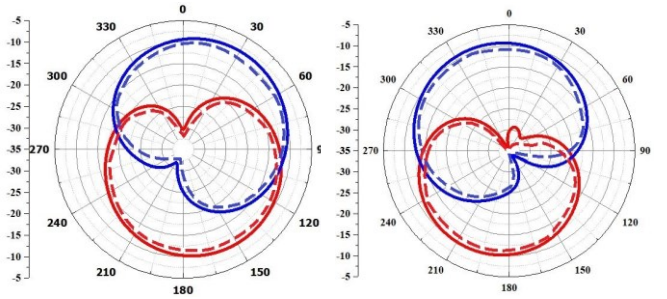

(a)

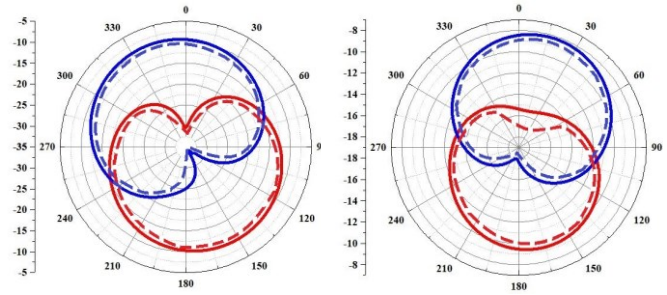

(b)

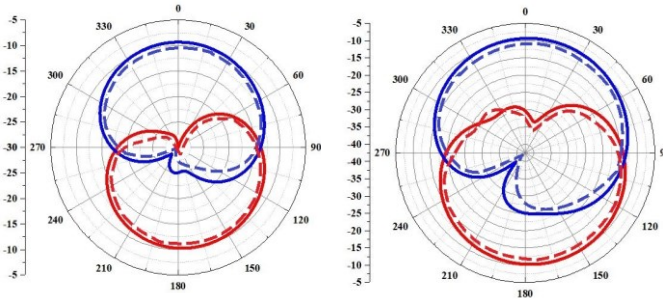

(c)

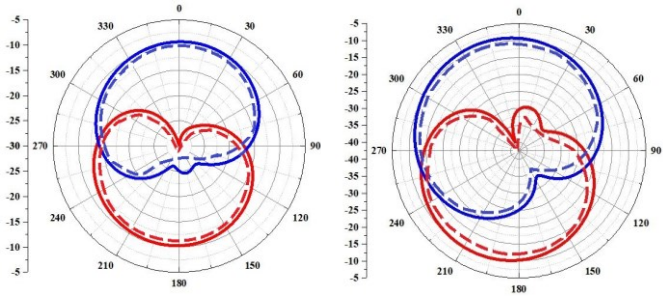

(d)

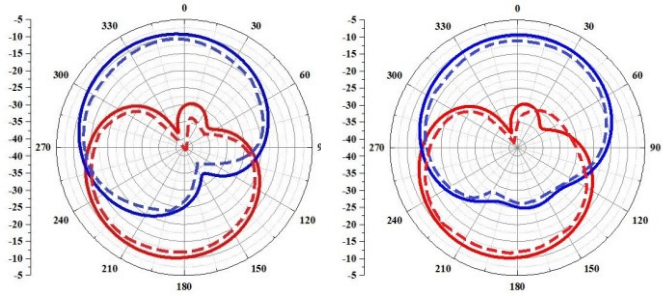

(e)

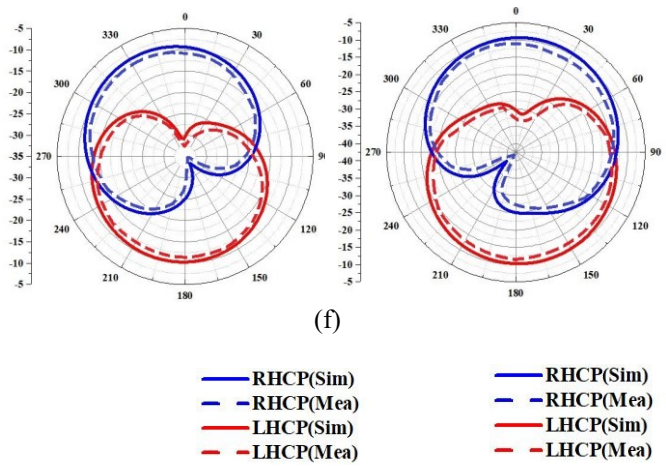

Fig. 10. Simulated cum Measured LHCP and RHCP of the exhibited antenna in E-H planes at frequencies (a)2.3 (b)3.6 (c)5.0 (d)5.3 (e)5.8 and (f)5.9 GHz

E. MIMO Performance Characteristics (TARC, ECC, DG, and Peak Gain).

The behavior of the proposed MIMO antenna is assessed with regards to envelope correlation coefficient (ECC), total active reflection coefficient (TARC), and diversity gain (DG), and peak gain by using equations (8, 9, and 10). The correlation between the two radiating elements in terms of mutual coupling can be studied by using ECC. ECC parameters can be evaluated by using the scattering parameters [9], as shown in equation 8. ECC should be very small to get better performance in the entire bandwidth. Ideally, ECC should be zero, but practically it's limit is less than (< 0. 5).

$$ECC = \frac{\left|S_{11}^{*}S_{12} + S_{21}^{*}S_{22}\right|^{2}}{(1-|S_{11}|^{2}-|S_{21}|^{2})(1-|S_{22}|^{2}-|S_{12}|^{2})} \quad (8)$$

$$DG = 10\sqrt{1-ECC^{2}} \quad (9)$$

Fig.11 shows the simulated and measured ECC evaluated using Reflection Coefficient and is less than 0.01, which indicates superior diversity characteristics for the MIMO antenna.

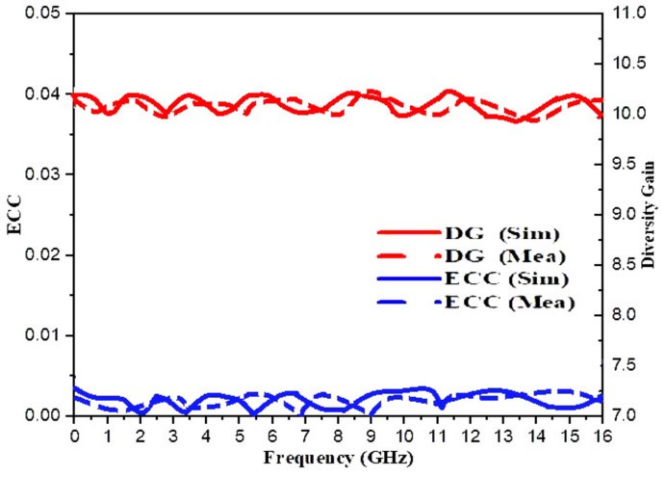

Fig. 11. ECC and DG of the multi-band MIMO antenna

The diversity gain of the proposed antenna can be evaluated by using equation 9. Fig.11 shows that the proposed antenna measured and simulated DG, which is higher than >9.5dB throughout the bandwidth. From the observed results, it shows that the proposed antenna has ECC lower than 0.01 and DG higher than 9.5. A decent correlation is attained between the simulated and measure values of the ECC and DG.

The overall operating bandwidth and efficiency of the system are greatly affected by the adjacent antenna radiating elements of the multi-port antenna system while operating simultaneously. So to predict the actual behavior of the system, solely depending on the s-parameters, is not enough. So, a new metric, TARC (total active reflection coefficient), is introduced. Fig.12 is measured as well as simulated TARC of the proposed antenna. The TARC of the MIMO antenna can be calculated by using equation 10 for dual or multi-ports. It is defined as the overall MIMO antenna return loss as taken as the square-root of the total reflected power by total incident power. The desirable value of TARC is less than -20dB, and the proposed antenna simulated and measured TARC values are illustrated in Fig.12, which are under -20 dB. Figure 13 exhibiting the simulated and measured peak gain of the proposed antenna, which is stable at 9dB at the operating band.

$$TARC = \sqrt{\frac{(S_{11}+S_{12})^{2}+(S_{21}+S_{22})^{2}}{2}} \quad (10)$$

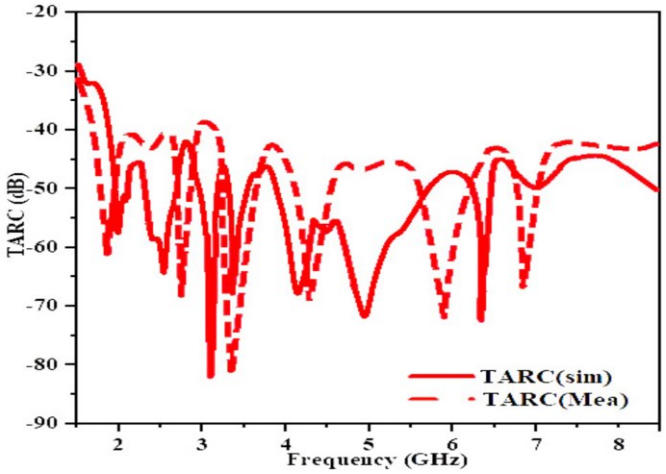

Fig. 12. TARC of the multi-band MIMO antenna

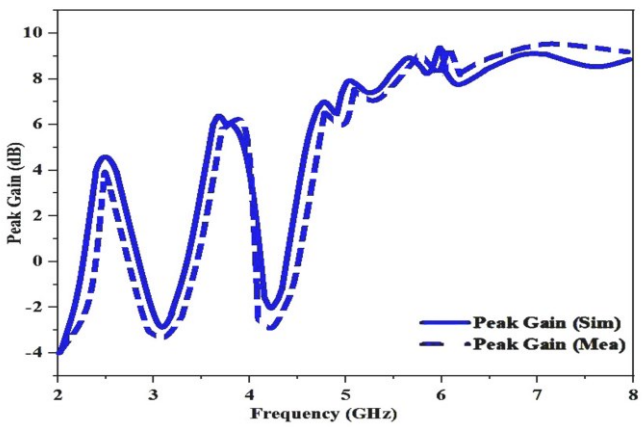

Fig. 13. Peak Gain of the multi-band MIMO antenna

TABLE II

COMPARING THE PROPOSED WORK WITH RECENTLY LITERATURE WORKS

Ref.No	Antenna Size (mm^2)	Reflection Coefficient (GHz)	Isolation (dB)	Gain (dB)	Circular polarization
[10]	30×40	3.0-10.6	-16	-	No
[11]	50×50	3.1-10.6	-15	Less than 2.8	No
[12]	48×48	2.7-10.7	-18	Less than 2.8	No
[13]	40×40	2.5-12	-15	3-6.7	No
[14]	34×49	3.4-12	-20	Stable 1.6	No
[15]	25×14	3.3-4.45	-	Stable 6	Yes
[16]	50×50	-	Above -17	-	Yes
Proposed Model	20×40	2.3- 9.2	-29	9	Yes

VI. CONCLUSION

A hybrid circularly polarized tapered-fed MIMO antenna with multi-band notched characteristics is proposed for Wi-MAX, Wi-Fi, Hyper LAN, ISM, and WLAN applications. Port isolation and bandwidth is improved by using the inverted L shaped structures in the ground plane. This advanced design achieved circular polarization with excellent performance in terms of radiation patterns, axial ratio, input matching, and better isolation below -20 dB, which demonstrate the high efficiency and robust performance of the MIMO antenna.

REFERENCES

[1] Shuai Zhang, and Gert Frolund Pedersen, "Mutual Coupling Reduction for UWB MIMO Antennas with a Wideband Neutralization Line," *IEEE Antenna Wireless Propag. Letters*, vol. 15, pp. 166-169, May 2016. https://doi.org/10.1109/LAWP.2015.2435992.

[2] Amjad Iqbal, Omar A. Saraereh, Arbab Waheed Ahmad, Shahid Bashir, "Mutual Coupling Reduction Using F-Shaped Stubs in UWB-MIMO Antenna," *IEEE Access*, vol. 6, pp. 2755-2759, Dec 2017. https://doi.org/10.1109/ACCESS.2017.2785232.

[3] Abdulrahman Shueai, Mohsen Alqadami, Mohd Faizal Jamlos, Ping Jack Soh, Guy A. E. Vandenbosch. "Assessment of PDMS Technology in a MIMO Antenna Array," *IEEE Antennas and Wireless Propagation Letters,* Volume: 15, 2016. https://doi.org/10.1109/LAWP.2015.2513960.

[4] Shraman Gupta, Zouhair Briqech, Abdel Razik Sebak, Tayeb Ahmed Denidni, "Mutual-Coupling Reduction Using Metasurface Corrugations for 28 GHz MIMO Applications," *IEEE Antennas and Wireless Propagation Letters* , Volume: 16, Pages: 2763 – 2766, DOP:25 August 2017. https://doi.org/10.1109/LAWP.2017.2745050.

[5] SeaheeHwangbo, Hae Yong Yang, Yong-Kyu Yoon "Mutual Coupling Reduction Using Micromachined Complementary Meander-Line Slots for a Patch Array Antenna," *IEEE Antennas and Wireless Propagation Letter*, vol. 16, pp. 1667 – 1670, 2017. https://doi.org/10.1109/LAWP.2017.2663114.

[6] Ullah, Ubaid, Ismail Ben Mabrouk, and Slawomir Koziel. "Enhanced-performance circularly polarized MIMO antenna with polarization/pattern diversity," *IEEE Access* Volume:8, 2020. https://doi.org/10.1109/ACCESS.2020.2966052.

[7] Amjad Iqbal, Amor Smida, Abdullah J. Alazani, Mohamed I. Waly, Nazih Khaddaj Mallat. "Wideband Circularly Polarized MIMO Antenna for High Data Wearable Biotelemetric Devices," *IEEE Access* Volume: 8, 2020. https://doi.org/10.1109/ACCESS.2020.2967397.

[8] K.G.Thomas and M.Sreenivasan, "A simple ultrawideband planar rectangular printed antenna with band dispensation," *IEEE Transaction on Antennas and Propagation*, vol. 58, no. 1, pp. 27–34, January 2010. https://doi.org/10.1109/TAP.2009.2036279.

[9] S. Blanch, J. Romeu, and I. Corbella, "Exact representation of antenna system diversity performance from input parameter description," *Electronics Letter*, vol. 39, no. 9, pp. 705–707, May 2003. https://doi.org/10.1049/el:20030495.

[10] J.-Y. Deng, L.-X. Guo, and X.-L. Liu, "An ultrawideband MIMO antenna with high isolation," *IEEE Antenna and Wireless Propagation Letters*, vol. 15, pp. 182–185, 2016. https://doi.org/10.1109/LAWP.2015.2437713.

[11] B. P. Chacko, G. Augustin, and T. A. Denidni, "Uniplanar polarization diversity antenna for ultrawideband systems," *IET Microwaves, Antennas & Propagation*, vol. 7, pp. 851–857, 2013. https://doi.org/10.1049/iet-map.2012.0732.

[12] P. Gao, S. He, Z. Xu, and Y. Zheng, "Compact printed UWB diversity slot antenna with 5.5-GHz band-notched characteristics," *IEEE Antenna and Wireless Propagation Letters*, vol. 13, pp. 376–379, 2014. https://doi.org/10.1109/LAWP.2014.2305772.

[13] J. Zhu, B. Feng, B. Peng, S. Li, and L. Deng, "Compact CPW UWB diversity slot antenna with dual band-notched characteristics," *Microwave and Optical Technology Letters*, vol. 58, no. 4, pp. 989–994, April 2016.

[14] H. Yoon, Y. Yoon, H. Kim, and C.-H. Lee, "Flexible ultra-wideband polarization diversity antenna with band-notch function," *IET Microwaves, Antennas & Propagation*, vol. 5, pp. 1463–1470, 2011. https://doi.org/10.1049/iet-map.2010.0126.

[15] J. Iqbal, U. Illahi, M. I. Sulaiman, M. M. Alam, M. M. Su'ud, and M. N. M. Yasin, "Mutual coupling reduction using the hybrid technique in wideband circularly polarized MIMO antenna for wimax applications," *IEEE Access*, vol. 7, pp. 40 951–40 958, 2019. https://doi.org/10.1109/ACCESS.2019.2908001.

[16] L. Qu, H. Piao, Y. Qu, H.-H. Kim, and H. Kim, "Circularly polarized MIMO ground radiation antennas for wearable devices," *Electronics Letters,* vol. 54, no. 4, pp. 189–190, 2018. https://doi.org/10.1049/el.2017.4348.